Preparation of ZrO_2/Al_2O_3-pillared Saponite and Its Spectroscopic Investigation on NO_X Adsorption

Is Fatimah[1]*, Karna Wijaya[2] and Narsito[2]

[1]Chemistry Department, Islamic University of Indonesia, Kampus Terpadu UII, Jl. Kaliurang Km. 14, Yogyakarta, Indonesia
[2]Chemistry Department, Gadjah Mada University, Sekip Utara, Yogyakarta

*Corresponding author: isfatimah@fmipa.uii.ac.id

Abstract: *Zirconia alumina (ZrO_2/Al_2O_3)-pillared saponite was prepared by the impregnation method using zirconium oxide chloride solution as a precursor. The effect of zirconia concentration on the physicochemical properties was studied with X-ray diffraction (XRD), surface area analysis and scanning electron microscopy (SEM). Its surface activity with respect to the change in physical properties was quantified by spectroscopic investigation of the adsorption of nitrogen oxide (NO_x). Significant differences were found in the material textural parameters with increasing zirconium (Zr) content, decreasing specific surface area and the formation of the monoclinic zirconia phase. It was found that zirconia dispersion contributed to the enhanced NO_x adsorption.*

Keywords: clay pillarisation, zirconia, dispersion, adsorption

1. INTRODUCTION

Pillared clays are semi-synthesised materials characterised as zeolite-like materials. The basic principle of preparation is exchanging charge compensating ions in the interlayer space of clay structures with the oligocation of hydrolysed metal followed by a calcination process to form a stable metal oxide. Due to its mechanism in the formation of pillars, pillared clays are porous materials that have high specific surface areas and exchangeable cations in pores. This property leads to their use as catalysts and solid supports of catalysts. Some investigations on pillared clay synthesis and applications for several chemical reactions have been reported[1–3]. Recent advances in clay modification include the use of pillared clays as solid supports for metal and metal oxide catalysts. For this purpose, relatively stable and reproducible pillared clays are needed. Among other metal oxides, a large number of papers are concerned with pillared clays (PILCs) with pillars of aluminium (Al). In addition to some reports of aluminium pillared clay applied as catalysts in several reactions, its use as a solid support is also reported by several authors.[3–6]

This work describes a new approach for pillared clays that act as supports for metal oxides. Aluminium pillared saponite was used as a matrix for zirconium dioxide (ZrO_2) dispersion. The physicochemical properties of samples with different zirconia contents were evaluated. In addition, the nitrogen oxide (NO_x) adsorption and reduction is reported.

2. EXPERIMENTAL

2.1 Material

Saponite mineral supplied by Kuninime Industry Co., Japan was used as the starting material. The cation exchange capacity (CEC) of the dry clay was estimated to be 98–120 meq/100 g. Al_2O_3-saponite was prepared using an aluminium chloride hexahydrate ($AlCl_3.6H_2O$) precursor supplied by Sigma Aldrich (Singapore) and NaOH supplied by E. Merck (Germany). Zirconium oxide chloride hydrate ($ZrOCl_2.8H_2O$) as a ZrO_2 precursor was also purchased from E. Merck. N_2 gas with ultra high purity (UHP) quality for calcination was supplied by Samator, Indonesia.

The Al_2O_3-saponite was prepared using the procedure previously reported.[7–8] A 5 g quantity of Al_2O_3-saponite powder (the particle size was 200 mesh) was diluted in distilled water, followed by stirring at room temperature for 1 h. Zirconium oxide chloride solution was added to the dispersion, and the mixture was stirred for 4 h. The solvent was evaporated at 50°C. The dry powder obtained was then calcined at 400°C for 4 h with a heating rate of 1°C–3°C/min. The concentrations of Zr in ZrO_2 precursor was 0.2, 0.6, 1.0 or 3.0 wt.%. The solid materials obtained were labelled as Zr/APS-concentration, for example, Zr/APS-0.6% indicating a Zr content of 0.6 wt.%. APS refers to Al_2O_3-saponite.

2.2 Characterisation

The phase analysis of saponite, APS and Zr/APS was carried out with a Shimadzu X6000 X-ray diffractometer using Cu Kα radiation, with an accelerating voltage of 40 kV and a current of 30 mA, scanned from 2θ of 5 to 70°. The optical absorption of the materials was determined using diffuse reflectance UV–visible spectroscopy measurements conducted with a JASCO V-760. The surface area and pore size were determined using a gas sorption analyser NOVA 1200e. The content of Zr in the samples was analysed by X-ray fluorescence (XRF) spectrophotometry. The major constituents of saponite and modified saponite were measured by an atomic absorption spectrophotometer from Perkin Elmer.

2.3 NO_x Adsorption and Reduction

NO_x adsorption was performed in a glass reactor. The dimensions of reactor were 10 cm in length with an inner diameter of 1 cm, placed inside a tubular furnace. Figure 1 shows the schematic diagram of the apparatus.

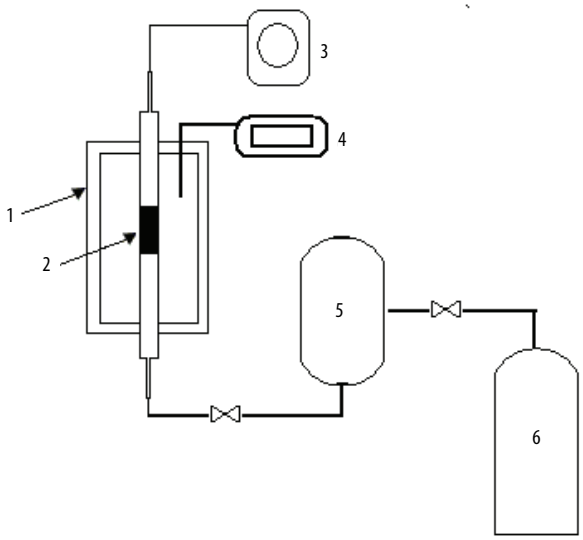

1. Furnace
2. Solid sample
3. Vacuum pump
4. Thermocontroller
5. NO_x chamber
6. N_2 gas

Figure 1: Scheme of NO_x adsorption apparatus.

A quantity of 3 g of sample powder was pelletised at a pressure of 7 tonnes and then placed in a solid sample holder inside the reactor. The reactor temperature was maintained at 200°C. NO_x adsorption was performed by flashing NO_x gas at a controlled flow rate of 1000 ppm/30 min using N_2 gas as a carrier. The sample was evacuated under a reduced pressure of 30 mmHg for 15 min before and after NO_x adsorption. To investigate the sample adsorptivity to NO_x, a small portion of the solid was collected to be analysed by Fourier transform infra-red (FTIR) spectroscopy immediately. To evaluate the qualitative adsorptivity to NO_x, 0.01 g of the collected solid was put in 100 ml Griess-Saltzman solution and 3% hydrogen peroxide (H_2O_2) followed by shaking for 3 h in order to leach the NO_x adsorbed on the sample surface and form the Griess-Saltzman complex. A pink colour appeared after the leaching, and the solution was measured with UV-visible spectrophotometry.

3. RESULTS AND DISCUSSION

3.1 Characterisation of the Prepared Materials

The chemical composition and cation exchange capacity (CEC) of APS compared to the raw saponite are presented in Table 1. The results show that the saponite consists of silicate and magnesium oxide. The existence of Al_2O_3 in APS material is due to the pillarisation process. The CEC decreases as the saponite interlayer cations are replaced by the Al_2O_3; however, APS has a CEC in the range of 39.90–45.90 meq/100 g, which indicates that it still provides sites for supporting cations.

Table 1: Chemical composition and cation exchange capacity (CEC) of saponite and APS.

Material	Chemical composition (wt.%)					CEC (meq/100g)	d_{001} (nm)
	SiO_2	Al_2O_3	Mg	Ca	Na		
Saponite	13.54	5.1	46.75	0.05	7.66	89.90–99.90	13.34
APS	10.52	23.72	35.78	0.01	0.25	45.5–49.5	15.79

Figure 2 shows the X-ray diffraction (XRD) patterns of APS and ZrO_2/APS. The patterns show a significant improvement in the saponite crystallinity after the pillarisation process. In agreement with the d_{001} data, the diffractogram shows the APS d_{001} reflection at $2\theta = 5.59^o$, corresponding to the height of the basal spacing, $d_{001} = 12.44$ Å, as previously reported.[7,8] The in-plane reflection (hkl) of the indices, independent of *c*-axis ordering, were observed at $2\theta = \sim 21.3^o$ in all samples. A weak peak at $2\theta = \sim 63.5^o$ corresponds to the amorphous silica structure. The d_{001} reflection suggests that the dispersion of ZrO_2 into the APS results in a decrease in intensity. The acidic environment created during the impregnation step is responsible for the delaminated pillared saponite structure. The results are in agreement with those previously reported[9] in the synthesis of titanium (Ti) pillared clays and the dispersion of TiO_2 in an aluminium pillared saponite matrix.

In addition, the difficulty of detecting the ZrO_2 phase in Zr/APS samples with Zr contents of 0.2%–0.6% indicates that zirconia aggregation is not formed at low Zr concentrations. On the other hand, a significant peak corresponding to the monoclinic zirconia phase is found in Zr/APS-1.0% and Zr/APS-3.0%, probably due to rapid hydrolysis at high concentrations of Zr precursor. Rapid hydrolysis of zirconia precursor was followed by zirconia deposition on the surface before it was dispersed in the pores of the matrix.

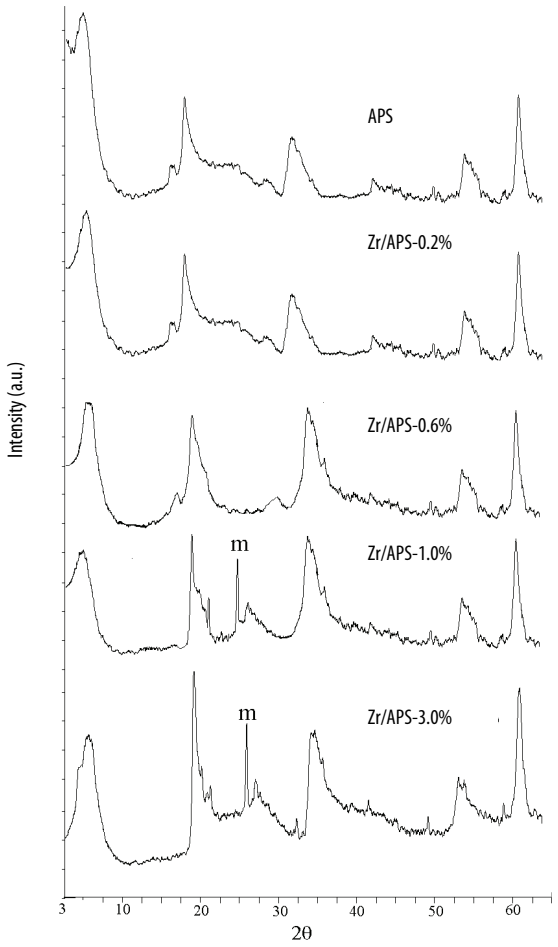

Figure 2: XRD patterns of the samples.

Note: m represents monoclinic reflection

Table 2 shows the relative crystallinity (d_{001}), Brunair-Emmet-Teller (BET) surface area and Zr content of the samples. At high concentrations of ZrO_2, the pore structure evolution was observed. This is confirmed by the adsorption-desorption isotherm profiles and the pore distribution graphs in Figures 3 and 4, respectively.

Although the relationship between the concentration of ZrO_2 supported in APS was not linear, the decreasing specific surface area was assumed to be the result of ZrO_2 incorporation in the spaces between pillars that caused aggregation. It was also found that the pattern of the adsorption/desorption curves were type IV by the Brunair-Deming-Deming-Teller (BDDT) classification, and,

consequently, mesopores prevailed in the pore structure of the systems. In correlation with the XRD pattern data, the possibilities for this condition are the destruction of the aluminium pillared clay framework or zirconia particle blocking in the pores, forming aggregates on the solid surface.

Table 2: Specific surface area, relative crystallinity and Zr content of material.

Material	Specific surface area (m^2/g)	Relative crystallinity (%)	Zr content (wt.%)
APS	269.76	100.00	–
Zr/APS-0.2%	232.58	96.81	0.1667
Zr/APS-0.6 %	227.68	92.55	0.4989
Zr/APS-1.0%	241.11	86.54	0.9876
Zr/APS-3.0%	244.42	73.18	0.3122

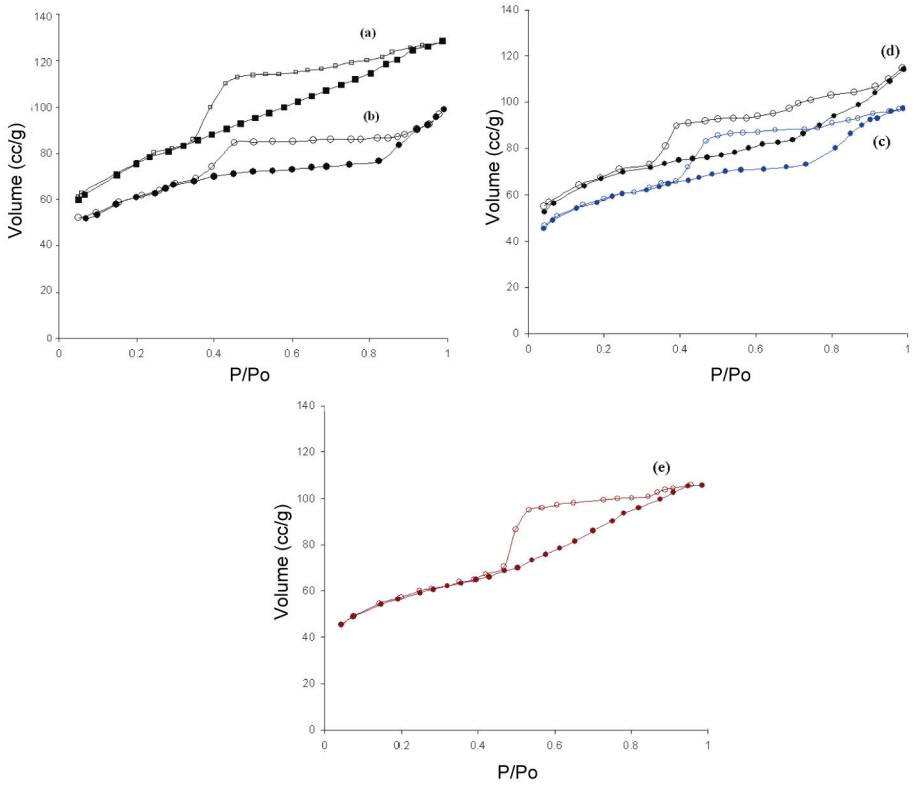

Figure 3: Adsorption-desorption profile of (a) APS, (b)–(e) Zr/APS 0.2% to 3%.

Note: P/Po: relative pressure

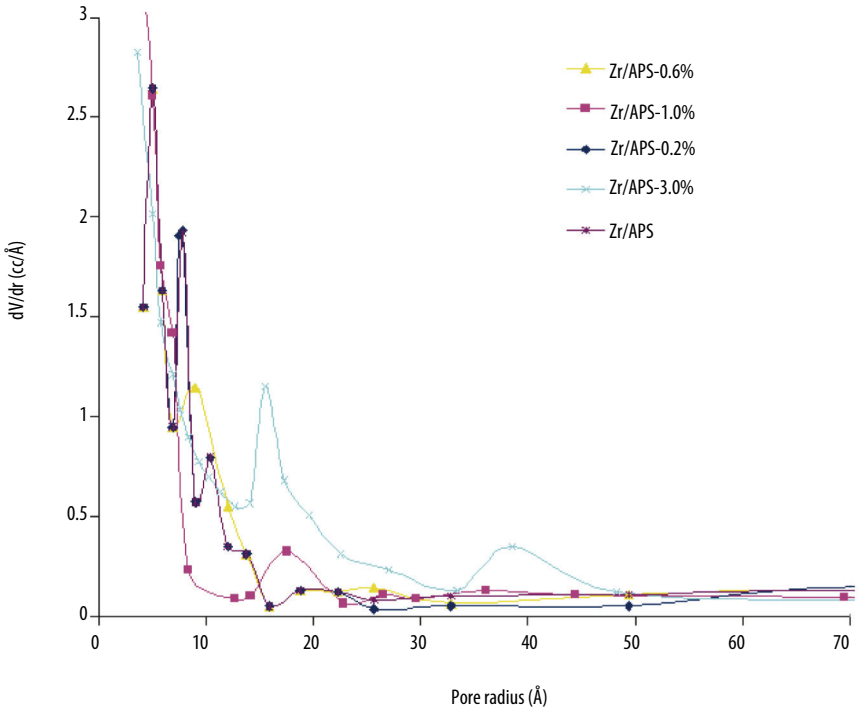

Figure 4: Barret-Joyner-Halenda (BJH)-pore distribution of the samples.

To ascertain the zirconia formation in the matrix, diffuse reflectance UV (DRUV)-visible and scanning electron microscopy (SEM) analyses were carried out. Figure 5 depicts the DRUV-visible spectra of Zr/APS materials compared to the APS. The UV–vis diffuse reflectance absorption spectrum of Zr/APS materials lies between the spectrum of APS and that of bulk-ZrO_2. The blue shift of the edge wavelength of Zr/APS is estimated to be in the range of 215–250 nm, suggesting nano size zirconia formation in the APS matrix. The character of spectra indicates the formation of monoclinic metaphase of zirconia particles. This pattern is in agreement with the XRD pattern in that, although the monoclinic phase in Zr/APS-3.0% is appreciable, the shift of the spectrum edge is the lowest one compared to the other Zr/APS samples. This justifies the aggregation hypothesis at high concentrations of Zr precursor. Moreover, SEM images in Figure 6 show the characteristics of Zr/APS-3.0% compared to the APS and Zr/APS-0.2%.

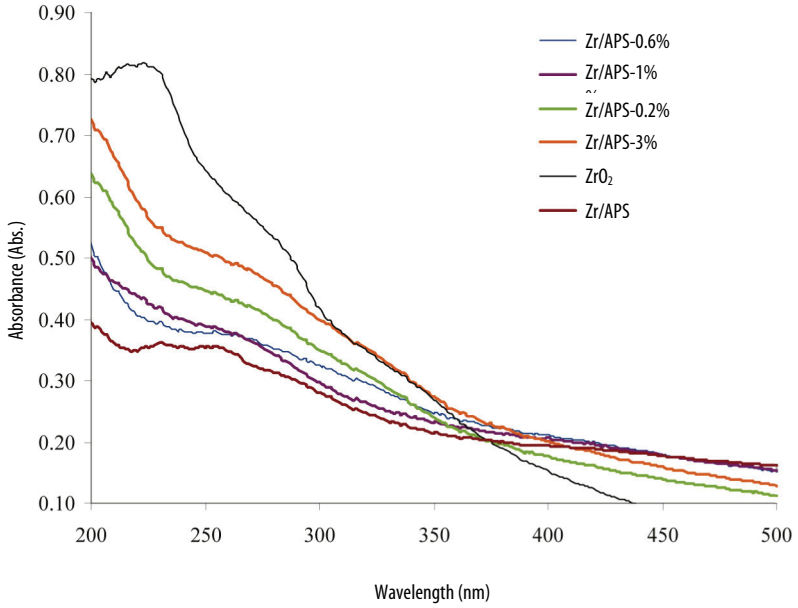

Figure 5: DRUV-visible spectra of the samples.

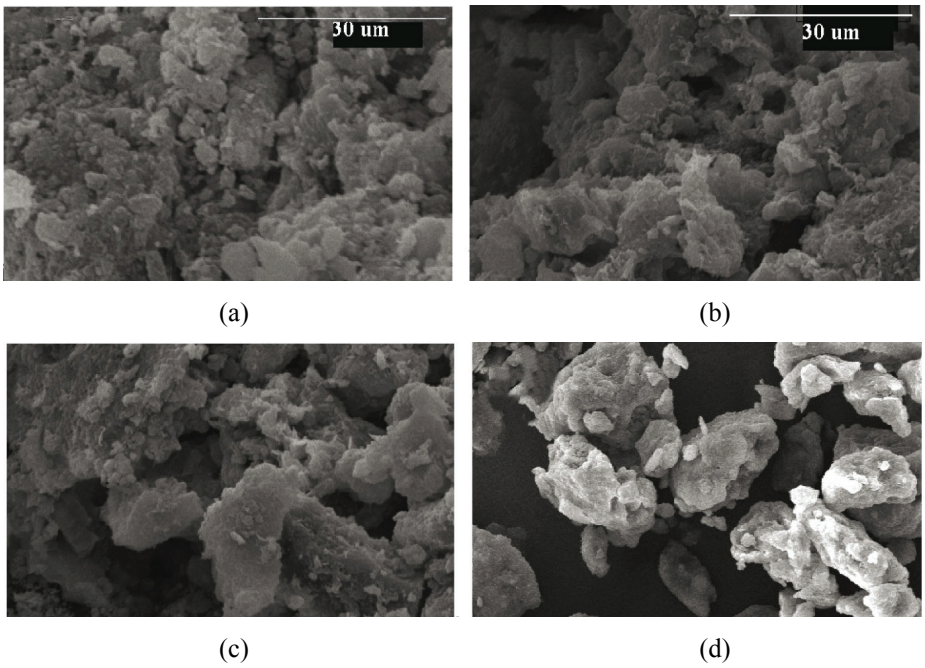

Figure 6: SEM profile of (a) APS, (b) Zr/ASP-0.2%, (c) Zr/APS-0.6%, (d) Zr/APS-3.0%.

3.2 NO_x Adsorption

In order to explain the effect of ZrO_2 dispersion on the surface activity, NO_x adsorption experiments were carried out. FTIR spectra of NO_x adsorbed materials were presented in Figure 7. The typical adsorption bands corresponding to the saponite structure are identified in the region of 1012.69 cm^{-1} and 661 cm^{-1} as the vibrations of the tetrahedral and octahedral sheet. The band at 462 cm^{-1} corresponds to Si-O-Mg in clay sheets, Si(Al)-O. A similar band at ~ 661 cm^{-1} was found in all ZrO_2/APS. The shifting band in this region can be ascribed to the Al-O bond that is tetrahedrally coordinated in the interlayer space exhibited by the pillarisation process. A broad band in the region around 3446 cm^{-1} indicates the adsorbed water (H_2O) in the pores of the solid. The shift of the band at ~ 660–690 cm^{-1} indicates the interaction between ZrO_2 and the Al-O of the metal oxide pillar. It can be seen that ZrO_2 dispersed in the solid exhibits a wave number shift to the left in this region. It is predicted that the interaction is responsible for increasing the vibrational energy.

The evidence of the chemisorption interaction of the surface with NO_x is shown by several spectra at ~ 1380 cm^{-1}, 1630 cm^{-1} and 2359–2345 cm^{-1}. These observed spectra are in agreement with those reported by several authors[10–12]. The adsorption of NO_x on all samples occurs through disproportionation, leading to the formation of nitrous acid, H_2O molecules, nitro species and anionic nitrosyls, NO^-. It corresponds to some of the characteristics for NO + O_2 species. Important spectra are the indication of NO_2 and NO_3 on the surface. The vibration at 1558.1 cm^{-1} is weakly observed in NO_x-adsorbed Zr/APS-0.2% and Zr/APS-0.6%, but is not present in other ZrO_2/APS samples. On the other hand, a sharp vibration peak at ~ 1384.32 cm^{-1} is observed in all samples. The vibration peaks at ~ 1560 cm^{-1} and 1380 cm^{-1} indicate that the NO_3 and NO_2 are adsorbed on the surface, respectively. This shows that NO_3 formed during adsorption is produced by ZrO_2 at low concentrations. This may be related to the homogeneous dispersion and high surface area of ZrO_2 that cause interaction between H_2O in air and NO_x to produce HNO_3. The interaction of Al-O and NO can be detected by the presence of the vibration spectrum (ν_s) at 1634.2 cm^{-1}.

Spectroscopic analysis of the Griess-Saltzman solution obtained by contacting NO_x on the solid surface with Griess-Saltzman reagent is presented in Figure 8. This qualitative method was adapted from the ASTM D1607 procedure.[13] The same amount of NO_x adsorbed solid was oxidised and then diluted in Griess-Saltzman reagent containing N-(1-naphthyl)ethylenediamine dihydrochloride, which is specifically reacted with NO_2 to produce a pink solution.

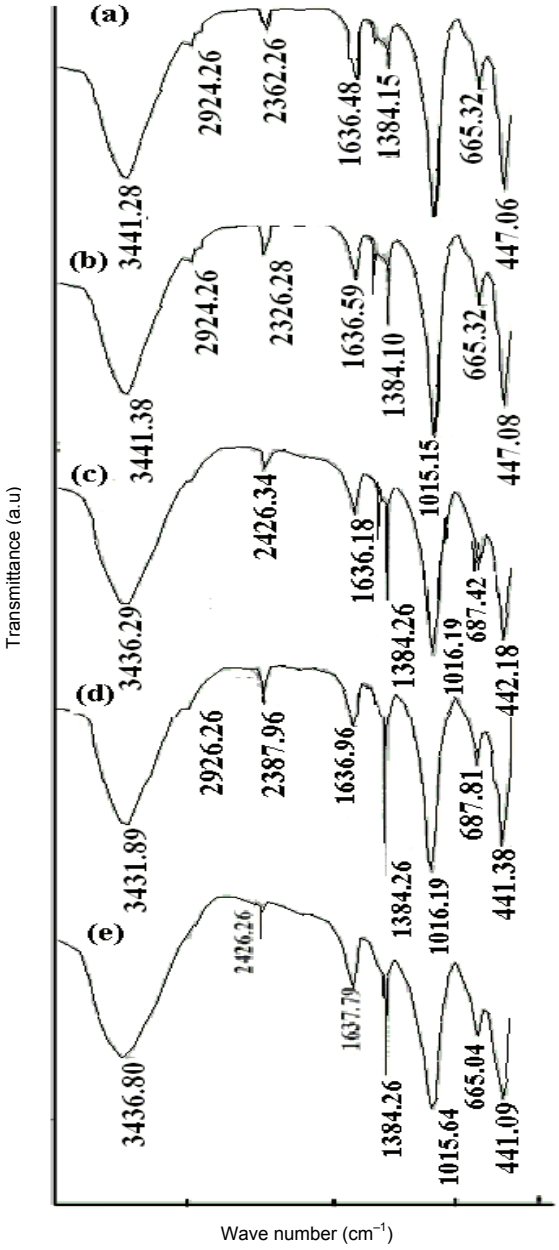

Figure 7: FTIR spectra of NO_x-adsorbed (a) APS, (b)–(e) Zr/APS 0.2% to 3%.

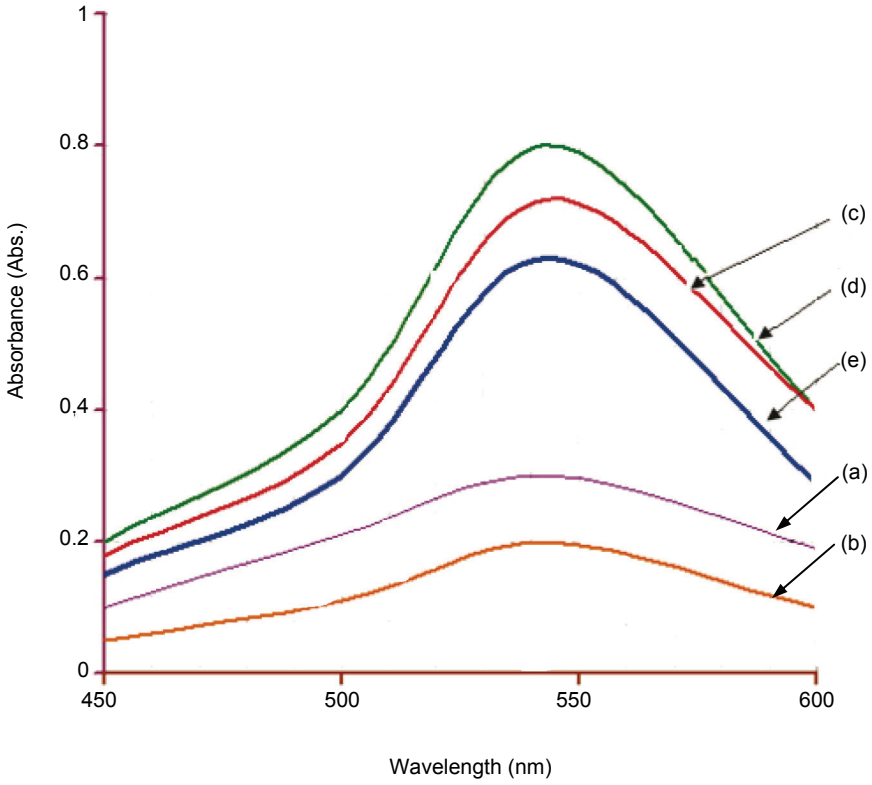

Figure 8: Spectra of Griess-Saltzman complex solution produced by dillution (a) APS, (b)–(e) Zr/APS 0.2%–3.0%.

Spectra of Griess-Saltzman solution were used to predict NO_x chemisorption on the surface at a maximum wavelength of 543.5 nm for the Griess-Saltzman complex. Based on absorption data, the adsorptivity of NO_x is increased in the following order: APS < ZrO_2/APS-0.2% < ZrO_2/APS-0.6% < ZrO_2/APS-3.0% < ZrO_2/APS-1.0%. A comparative investigation on the adsorptivity of ZrO_2/APS-3.0% and ZrO_2/APS-1.0% samples was done in order to study the role of zirconia dispersion in the APS matrix. From the DRUV-vis spectra and SEM images, it is clear that the zirconia in ZrO_2/APS-3.0% is not homogeneously dispersed. This is the reason for the ineffective interaction between NO_x and the surface.

4. CONCLUSION

ZrO_2 has been successfully dispersed in aluminium pillared saponite through the impregnation method with zirconia pillaring precursor. Investigation of the effects of the zirconia content on the physicochemical properties showed that it had a tendency to reduce the specific surface area and crystallinity. The aggregation of the monoclinic zirconia phase was identified in the sample with Zr content > 1 wt.%. Furthermore, the spectroscopic investigation study showed that zirconia dispersion improved the adsorptivity to NO_x. The adsorptivity seems to be controlled and closely related to the homogeneity of the dispersion.

5. ACKNOWLEDGEMENTS

The authors gratefully acknowledge Kuninime Ind. Co. Japan for saponite specimens and Arif Hidayat, M. Eng and Khoirul Himmi, S. Si for laboratory assistance.

6. REFERENCES

1. Gil, A., Gandia, L. & Vicente, M. A. (2000). Recent advances in the synthesis and catalytic applications of pillared clays. *Catal. Rev. Sci. Eng*., 42(1&2), 145–212.
2. Guelou, E., Barrault, J., Fournier, J. & Tatibouet, J. M. (2003). Active iron species in the catalytic wet peroxide oxidation of phenol over pillared clays containing iron. *Appl. Catal. B*, 44(1), 1–8.
3. Hernando, M. J., Pesquera, C., Blanco, C. & Gonzalez, F. (2001). Synthesis, characterization, and catalytic properties of pillared montmorillonite with aluminum/cerium polyoxycations. *Chem. Mater*., 13(6), 2154–2159.
4. Bahranowski, K., Gasior, M., Kielski, A., Podobinski, J., Serwicka, E. M., Vartikian, L. A. & Wodnicka, K. (1998). Physico-chemical characterization and catalytic properties of copper-doped alumina-pillared montmorillonites. *Clays Clay Miner.,* 46(1), 98–102.
5. Wang, J., Merino, J., Aranda, P., Galvan, J. C. & Ruiz-Hitzky, E. (1999). Reactive nanocomposites based on pillared clays. *J. Mater. Chem*., 9(1), 161–168.
6. Nachtegaal, M., Scheidegger, A. M., Dähn, R., Chateigner, D. & Furrer, G. (2005). Immobilization of Ni by Al-modified montmorillonite: A novel uptake mechanism. *Geochim. Cosmochim. Acta*, 69(17), 4211–4225.
7. Fatimah, I., Narsito & Wijaya, K. (2009). Controling factor in synthesis of aluminium pillared saponite and aluminium pillared montmorillonite. *Indonesian J. Chem.*, 9(1), 6–11.

8. Fatimah, I., Wang, S., Narsito & Wijaya, K. (2008). A comparative study on aluminium pillared smectite synthesis from synthetic saponite and indonesian montmorillonite. *Asean J. Chem. Eng.*, 8(1), 69–77.
9. Yuan, P., Yin, X., He, H., Yang, D., Wang, L. & Zhu, J. (2006). Investigation on the delaminated-pillared structure of TiO_2-PILC synthesized by $TiCl_4$ hydrolysis method. *Micro. Meso. Mat.,* 93(1–3), 240–247.
10. Valverde, J. L., Lucas, A., Dorado, F., Romero, A. & Garcia, P. B. (2005). Study by in situ FTIR of the SCR of NO by propene in Cu^{2+} ion-exchanged Ti-PILC. *J. Mol. Catal. A: Chem.,* 230, 23–28.
11. Hadjiivanov, K., Avreyska, V., Klissurski, D. & Marinova, T. (2002). Surface species formed after NO adsorption and NO + O_2 coadsorption on ZrO_2 and sulfated ZrO_2: An FTIR spectroscopic study. *Langmuir*, 18(5), 1619–1625.
12. Kantcheva, M. & Ciftlikli, E. Z. (2002). FTIR spectroscopic characterization of NO_x species adsorbed on ZrO_2 and ZrO_2−SO_4^{2-}. *J. Phys. Chem. B*, 106(15), 3941–3949.
13. Lodge, J. (1986). *Methods of air sampling and analysis* (pp. 389). Washington DC: APA.